



Research paper

Versatile gold based SERS substrates fabricated by ultrafast laser ablation for sensing picric acid and ammonium nitrate



Chandu Byram, Sree Sathya Bharathi Moram, Abdul Kalam Shaik, Venugopal Rao Soma*

Advanced Center of Research in High Energy Materials (ACRHEM), University of Hyderabad, Prof. C. R. Rao Road, Hyderabad 500046, India

ARTICLE INFO

Article history:

Received 14 June 2017

In final form 18 July 2017

Available online 20 July 2017

ABSTRACT

We demonstrate the detection of picric acid (PA) and ammonium nitrate (AN) at μM concentrations by utilizing gold (Au) nanostructures (NSs) as surface enhanced Raman scattering (SERS) substrates fabricated using the technique of ultrafast laser ablation in liquids. Au NPs and NSs were also utilized for detecting Rhodamine 6G (Rh6G) and methylene blue (MB). Detection of all the molecules using the same substrates (NPs and NSs) demonstrated their versatility. Detection limits of 10^{-5} , 10^{-6} , 10^{-7} , 10^{-8} M were achieved for AN, PA, Rh6G and MB, respectively. Reproducibility of the SERS intensity using NSs and NPs as substrates demonstrate their efficacy.

© 2017 Elsevier B.V. All rights reserved.

1. Introduction

Security at the national borders as well as homeland security is the prime concern of any state owing to terrorism and international activities. The extensive open literature available on explosive chemistry and easy procurement of unrestricted precursors has certain conduit to “homemade” explosives or IEDs (improvised explosive device) which comprises an oxidizer along with an initiation system [1]. Picric acid (PA) is itself an explosive, easily synthesized from freely available precursors and prone to be used in IEDs [2]. Ammonium Nitrate (AN, common organic fertilizer) is exploited in manufacturing of IEDs by insurgents as it is a good oxidizer, easily accessible and cheap. However, the detection and identification process of such explosives is a tedious job owing to their low sensitivity and the matrix effects of the sample. Despite numerous laser based techniques available to detect or identify explosives [3,4], surface enhanced Raman scattering (SERS) has attracted increasing attention in research community due to its high selectivity, sensitivity and fingerprint nature. SERS has enormous potential for applications in the fields of biological sensing [5] and explosive detection [6–8]. SERS is a surface sensitive technique which enhances the Raman signal from analyte molecules adsorbed on roughened metal nanostructure (NS)/nanoparticle (NP) surface. In SERS, two mechanisms are responsible for the enhancement in Raman signals viz. electromagnetic (EM) and chemical mechanism (CM) [9,10]. Considerable efforts have been devoted for fabricating efficient SERS substrates with high sensitivity, reproducibility, stability combined with low cost [11–13]. In

general, plasmonic metals (Ag, Au, and Cu) are frequently used as SERS substrates because of their superior plasmonic nature in the visible range. Compared to silver and copper, gold provides high stability with a lower oxidation tendency. Due to exceptional optical and electronic properties, gold nanomaterials have garnered attention in various fields explicitly in imaging, sensing [14]. Numerous methods have been developed to fabricate gold NPs including seed growth method, citrate reduction method etc. Further advancements in the area of photonics and nanotechnology has paved the way for fabrication of several patterned and nano textured lithographic substrates with Ag, Au coating. However, these fabrication methods involves multiple stages, various mechanisms, sophisticated instruments and consume more time [15]. In comparison with prior mentioned methods, ultrafast laser ablation in liquids (ULAL) has emerged as promising technique to synthesize green NSs/NPs of pure metal, semiconductors and core-shell NPs by ablating Alloy or irradiating mixed colloidal solutions in a single step [16–20]. These NPs are pure, less toxic, ligand free and void of reducing agents, and thus efficaciously used in various fields such as SERS, LDA-MS, catalysis, bio-medicine and optical limiting devices [14]. The LAL NPs produced by changing laser parameters and fabrication process result in different shapes, size and clusters (nano chains, nano triangles, etc.) and these are exploited in SERS owing to induction of high electric fields at their edges/tips [14,21]. Earlier reports demonstrated the superior nature of LAL NPs over the chemically synthesized NPs with superior SERS response, clean background in Raman spectra and high reproducibility [14,22,23]. Recently, novel nanomaterials such as (i) aggregates of Plasmonic NPs mixed with magnetic NPs for SERS and cell imaging [24,25] (ii) plasmonic NPs capable of self-assembly [26,27] (iii) Plasmonic NPs decorated composite

* Corresponding author.

E-mail address: soma_venu@yahoo.com (V.R. Soma).

graphene films are being fabricated [28]. Though these entities exhibited higher SERS performance, their stability is still under investigation. Besides these NPs, super hydrophobic NSs with diverse morphology fabricated by LA technique could be exploited to detect ultra-trace levels of analyte [29]. In this study, we report the detection of PA, AN, Rhodamine 6G (Rh6G) and methylene blue (MB) using Au NSs and PA, Rh6G, MB using Au NPs as SERS substrates, fabricated by ULAL technique. To the best of our knowledge, this is the first report on the detection of PA and AN using ULAL fabricated Au NSs.

2. Experiments

NSs and NPs were achieved through the ULAL technique using a femtosecond (fs) amplifier (LIBRA, coherent) delivering ~ 50 fs pulses at a central wavelength of 800 nm. The laser was focused using a convex lens of 100 mm focal length at normal incidence on to the bulk gold target ($10 \times 10 \times 1$ mm³) immersed in distilled water and placed in a glass beaker. The liquid layer height above the target surface was ~ 13 mm. The glass beaker was mounted on X-Y motorized stage (Newport) and translated with 500 μ m/s speed in both directions to produce NSs on a target of 5×5 mm². The typical ablation time was ~ 20 min for the scanning and the estimated beam waist on target surface was ~ 100 μ m. The ablation experiments were performed with varying pulse energies of ~ 200 , ~ 300 , ~ 400 and ~ 500 μ J. The prepared Au NPs and NSs are labelled as AuNP1, AuNP2, AuNP3, AuNP4 and AuNS1, AuNS2, AuNS3 and AuNS4 for input energies of ~ 200 , ~ 300 , ~ 400 and ~ 500 μ J, respectively. The optical absorption studies were performed with UV–Visible spectrometer in 250–800 nm wavelength range. Morphological studies of the NPs were investigated by transmission electron microscope (TEM). Surface morphology of NSs was characterized by field emission scanning electron microscope (FESEM). In all the SERS measurements (NPs/NSs), Rh6G was probed with 532 nm (micro-Raman spectrometer, WITec Alpha-300) and PA, MB were probed with 785 nm (portable Raman spectrometer, B&W Tek) and AN was probed with 632 nm (Micro Raman, HORIBA) with an integration time of 5 s.

3. Results and discussion

The surface plasmon resonance (SPR) peaks of the colloids were observed near 530 nm and the width of SPRs changed with the input pulse energy. The SPR position is primarily dependent on the shape and size of the nanoparticles [30,31]. The absorption of NPs increased with the laser energy due to the higher ablation yield. The shape, size and crystallinity of obtained NPs were investigated by transmission electron microscope (TEM). Fig. 1(a)–(d) illustrates the TEM images of AuNP1, AuNP2, AuNP3, and AuNP4. Polydispersity of NPs is evident and most of the NPs are in spherical shape with smaller diameters (3–15 nm) along with co-existing larger particles (>40 nm). From the statistical analysis, the measured mean sizes were ~ 13.6 , 7.6, 6.5 and 6.2 nm (data presented in Fig. S1 of supporting information) for AuNP1, AuNP2, AuNP3, and AuNP4, respectively. The observed mean sizes of NPs decreased with increasing laser energy [32].

The chain-like structures observed in TEM images could be attributed to the laser induced agglomeration (LIA) which arises due to the non-equilibrium charge distribution among Au NPs. As suggested by Serkov et al., two-photon absorption or thermionic emission are the two plausible mechanisms for the ionization of Au NPs. The dipole interactions and electrostatic balance between the ionized Au NPs and neutral atoms lead to the formation of chain-like structures on eventual laser irradiation [26,33]. Fig. 2 (a)–(d) illustrates the FESEM images of laser machined portions of AuNS1, AuNS2, AuNS3 and AuNS4 respectively. Different ran-

dom morphologies of nanostructures along with nanopores and nanorims on AuNS1 [Fig. 2(a)], nanodroplets of irregular shape and size on AuNS2 [Fig. 2(b)], nanodroplets on AuNS3 [Fig. 2(c)] and nano-protrusions on AuNS4 [Fig. 2(d)] were observed. The complex interaction of fs pulses with the metal surface, involving melting of target, cavitation bubble formation and re-deposition of ablated material back on to the surface could have resulted in nanopores, nanocavities and nanorims [34,35]. This conjecture of NSs morphology could be described by the two-temperature model (TTM), where energy coupling between electrons and lattice phonons with fs excitation are considered [36]. In the first case, NPs were chosen as a SERS platform for the identification of Rh6G, MB and PA. 20 μ L of NP colloidal solution from AuNP1, AuNP2, AuNP3 and AuNP4 was placed on individual Si substrates, then dried on hot plate at 50 $^{\circ}$ C to form a layer (film). Later a tiny drop (20 μ L) of Rh6G (150 nM) was placed on individual NP layers (film) and allowed to dry.

Fig. 3(a) presents the Raman spectra of Rh6G (150 nM) adsorbed on AuNP1 (black), AuNP2 (red¹), AuNP3 (blue) and AuNP4 (magenta) layers. From the SERS spectra [Fig. 3(a)], the major Raman peaks of Rh6G were identified at 612, 780, 1180 cm^{-1} assigned to C-C ring in plane bend, C-H out plane bend, C-C stretch while the 1315, 1356 1650 cm^{-1} peaks are attributed to the aromatic C-C stretch. Normal Raman spectra of Rh6G (0.25 M) and MB (0.1 M) were recorded on bare Si substrate. The enhancement factors (EFs) were estimated by considering the prominent mode of Rh6G (1365 cm^{-1}) observed from Au NP films (NPs drop casted on Si) with that of normal Raman spectra recorded from the Si substrate. The EFs were evaluated by adopting the procedure (Eq. (1)) [37].

$$EF = \frac{I_{\text{SERS}}}{I_{\text{Raman}}} \times \frac{N_{\text{Raman}}}{N_{\text{SERS}}} \quad (1)$$

where I_{SERS} is the integrated intensity of elevated vibrational mode of analyte from the NS/NP, I_{Raman} is the intensity of same mode obtained from Si substrate, N_{SERS} and N_{Raman} are the number of molecules contributing towards the SERS and Raman signals.

For Rh6G (1365 cm^{-1}), the estimated EFs were 6.6×10^5 , 9.6×10^5 , 7×10^5 and 1.4×10^6 for AuNP1, AuNP2, AuNP3 and AuNP4, respectively. The reproducibility of Au NP was investigated by collecting the SERS spectra of Rh6G at various positions on NP films (drop casted) [data presented in Fig. 3(b)]. The variation in the SERS intensity was estimated to be <20%. In earlier reports, Hui He et al., demonstrated that the Au chains fabricated by LAL technique exhibited superior SERS performance for detecting Rh6G at nM concentration assisted by electrophoretic deposition on to the other substrate which is comparable with our detection of Rh6G [38]. Fig. 3(c) shows the SERS spectra of MB (50 nM) recorded from AuNP1, AuNP2, AuNP3 and AuNP4 films using 785 nm laser excitation. The predominant mode of MB located at 1621 cm^{-1} is attributed to the C-C ring stretching. The other modes observed were at 449 cm^{-1} , 505 cm^{-1} which correspond to the C-N-C skeletal deformation, 590 cm^{-1} (skeletal deformation of C-S-C), 667 cm^{-1} (out of plane bending of C-H), 766 cm^{-1} (in-plane bending of C-H), 1040 cm^{-1} (in-plane bending of C-H) and 1393 cm^{-1} (Symmetric stretching of C-N) [see Tables S1–S3 supporting information for complete details of assignments]. The data of the modes observed in the present case are consistent with the prior reports [39,40]. The estimated EFs (for the 1621 cm^{-1} peak) were 1.5×10^6 , 1.4×10^6 , 1.7×10^6 and 4.6×10^6 for AuNP1, AuNP2, AuNP3 and AuNP4, respectively.

Fig. 3(d) illustrates the Raman spectra of PA (5 μ M) adsorbed on AuNP1, AuNP2, AuNP3 and AuNP4 respectively. The prominent peaks of PA (in normal Raman spectra though not shown) were

¹ For interpretation of color in Fig. 3, the reader is referred to the web version of this article.

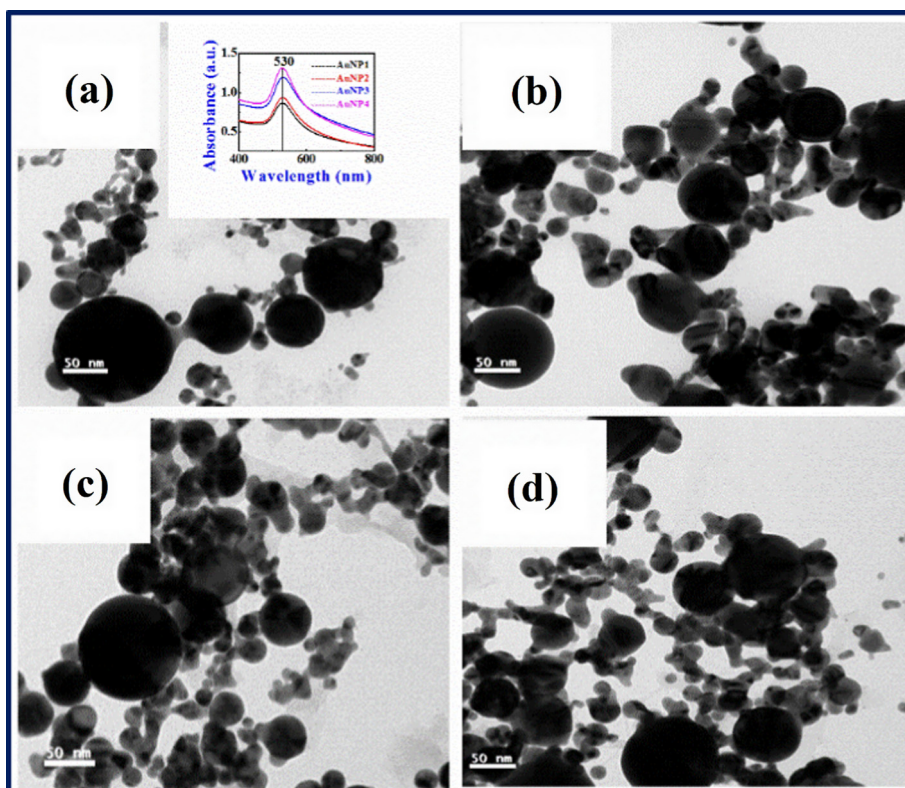


Fig. 1. TEM micrographs of (a) Au NP1, (b) Au NP2, (c) Au NP3 and (d) Au NP4 obtained with varying input laser energies. Inset of (a) depicts the UV–visible absorption spectra of all the nanoparticles obtained.

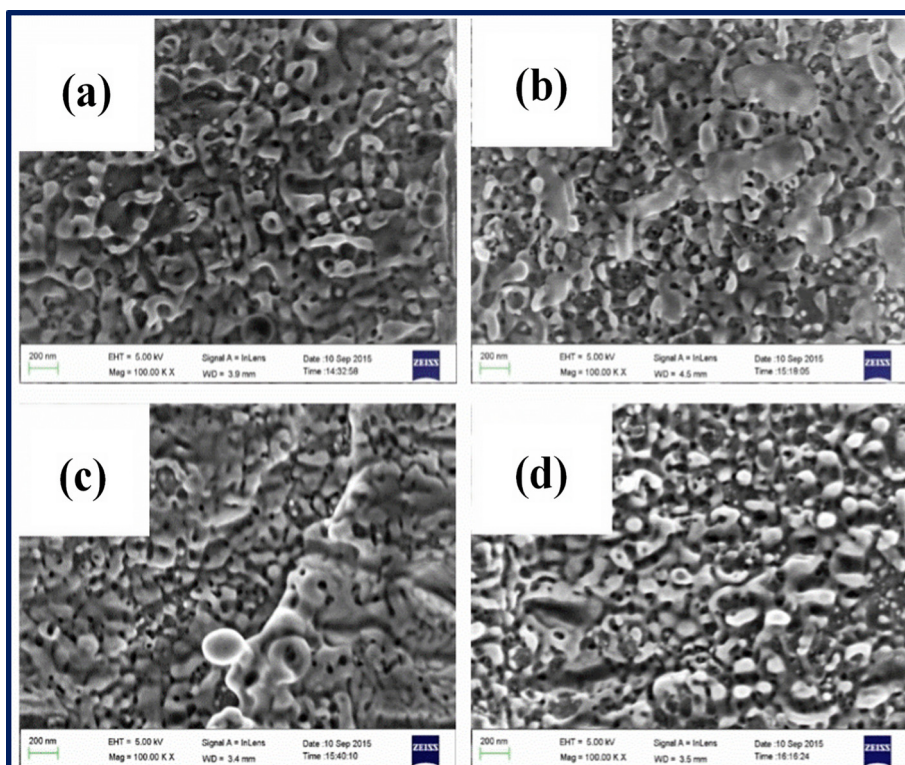


Fig. 2. FESEM images of laser ablated portions on (a) AuNS1, (b) AuNS2, (c) AuNS3 and (d) AuNS4 achieved at laser energies of 200, 300, 400 and 500 μJ respectively.

observed at 825 (C–H bending), 1175, and 1344 cm^{-1} (NO_2 symmetric stretching) [41]. However, in all SERS spectra 822 cm^{-1} mode of PA was still observed even at the concentration of

10^{-6} M on all NPs films [see Tables S1–S3 in supporting information for complete details of assignments]. The estimated EFs for the 822 cm^{-1} mode of PA were 3.8×10^4 , 3.9×10^4 , 3×10^4 and

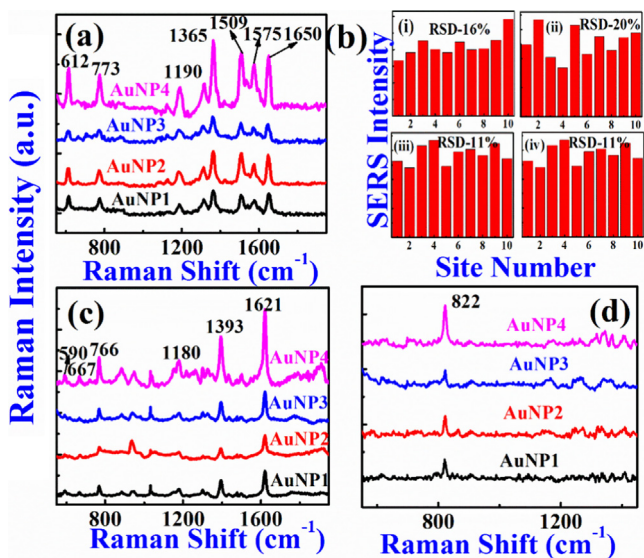


Fig. 3. (a) SERS spectra of Rh6G (150 nM) and (b) its reproducibility data for AuNP1, AuNP2, AuNP3, and AuNP4 using 532 nm excitation. SERS spectra of (c) MB (50 nM) and (d) PA (5 μ M) recorded from AuNP films (drop casted on Si) using a portable Raman spectrometer (785 nm excitation).

7.9×10^4 for AuNP1, AuNP2, AuNP3 and AuNP4, respectively. The observed EFs could be ascribed to the elevation of evanescent fields arising from the coupling of incident photons to localized surface plasmons at the NP surface [42]. NPs aggregation also could possibly affect EFs, as their distribution on substrate was random and not controllable (owing to drop casting) which led to the generation of substantial number of hotspots in their vicinity. In the second case, Au NSs were utilized as SERS substrates. SERS studies were performed for AN (50 μ M), PA (5 μ M), Rh6G (150 nM), and MB (50 nM) with the aim of demonstrating their versatility and reusability of these Au NSs after thorough cleaning with acetone and deionized water in an ultrasonic bath. Our group had earlier demonstrated the multiple use of Cu NSs for detection of various molecules using SERS technique [7]. For SERS studies, 20 μ L of each analyte was dropped on to the four NSs and allowed to dry.

Fig. 4(a) presents the SERS spectra of Rh6G (150 nM) recorded from Au NSs. For Rh6G estimated EFs were 3.6×10^5 , 5×10^5 , 4.8×10^5 and 9.5×10^5 for AuNS1, AuNS2, AuNS3 and AuNS4, respectively. The reproducibility of the enhancement factors in the case of NSs was also studied and it was found to be reasonably good over large areas [see Fig. S2 in supporting information]. Similarly, the SERS spectra of MB (50 nM) were acquired by utilizing the same substrates (for second time, after appropriate cleaning) and are presented in Fig. 4(b). The characteristic peaks of MB positioned at 448, 1393 and 1621 cm^{-1} with higher intensity and other modes with lower intensity were identified with the detection limit of 10^{-8} M using fabricated NSs. The calculated EFs of MB (for 1621 cm^{-1} mode) were 0.4×10^6 , 1×10^6 , 1.4×10^6 , and 1.5×10^6 for AuNS1, AuNS2, AuNS3 and AuNS4, respectively. Fig. 4(c) illustrates the Raman spectra of PA (5 μ M) recorded on Au NSs. The evaluated EFs for the 822 cm^{-1} mode of PA were 6.9×10^4 , 3.9×10^4 , 2.3×10^4 and 1.6×10^5 for AuNS1, AuNS2, AuNS3 and AuNS4 respectively. Fig. 4(d) illustrates the SERS spectra of AN (50 μ M) and EFs for the 1053 cm^{-1} (NO_3^- symmetric stretch) [43] mode of AN were 1×10^3 , 1.6×10^3 , 2×10^3 and 2.8×10^3 .

The diverse EFs observed for different analytes could be attributed to (i) the selective support offered by a NS/NPs to a molecule which depends on the adsorption, orientation [44] or settlement of analyte on the laser machined portions (ii) excitation wavelength [42] used (iii) size and shape of the NP/NS and the number of

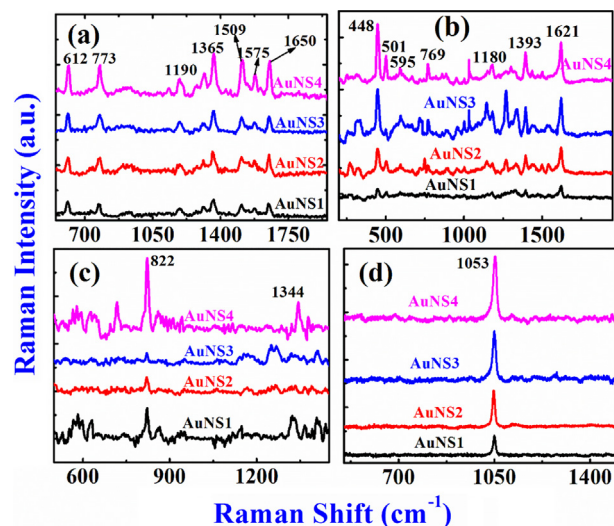


Fig. 4. SERS spectra of (a) Rh6G (150 nM), (b) MB (50 nM), (c) PA (5 μ M) and (d) AN (50 μ M) on all AuNSs using 532 nm (for Rh6G), 785 nm (for PA, MB) and 632 nm (for AN) excitations.

hotspots available [45]. NSs have exhibited superior SERS performance compared to NPs in case of explosives. As for portable and field applications, to the best of our knowledge, we strongly feel that our fabricated Au NSs are better SERS substrates compared to Au NPs as they are (i) easy to handle (ii) reusable after a simple cleaning procedure (iii) less oxidized over a period of time compared to NPs where oxidation dominates the agglomeration effect which diminishes the performance of NPs. Besides this, our NSs has shown comparable SERS performance with commercial substrates [46]. Sabina et al., have demonstrated the detection of explosives with EFs of 10^4 – 10^6 using Klarite commercial substrate [47]. Compared to commercial substrates (compact, single use and are to be opened just before the measurements) our substrates are easy to fabricate, can be used multiple times (using normal cleaning procedures) for detection of various analytes (explosives and dyes) and also achieved the EFs up to 10^6 which is comparable to the former substrates EFs [48]. We are exploring the possibility of increasing the enhancements through a simple procedure of placing the obtained NPs on the NSs thereby achieving higher number of hotspots [49]. In this endeavour, we have already achieved 5–6 times increase in the EF's by simply placing the NPs on the NSs (which is a very simple procedure). Further detailed studies are in progress to this extent. We have also established that using Bessel beam instead of Gaussian beam will improve the EF's [50]. Our goal is to achieve robust SERS substrates which can detect trace levels of all the common explosives using portable/hand-held spectrometer.

4. Conclusions

In summary, we have successfully demonstrated the versatile nature of the NSs fabricated using fs pulses for SERS based detection of AN, PA, Rh6G and MB. The EFs of $\sim 10^3$, $\sim 10^4$, $\sim 10^5$, and $\sim 10^6$ were achieved for AN, PA, Rh6G and MB, respectively, using these Au NSs. We have clearly demonstrated the main advantages of our SERS substrates: (a) recyclable and multipurpose nature (b) NPs and NSs both as SERS substrates (c) Multiple molecules detected using these substrates and (d) SERS spectra recorded with a portable Raman spectrometer, useful for practical and on-field studies (e) simple procedure for fabrication and cleaning of these substrates. Besides, we are also investigating the procedures to increase the observed EFs by combining NPs and NSs and

expanding the repertoire of these substrates by investigating other explosive molecules also.

Acknowledgments

We thank DRDO, India for continuous financial support. We also thank Centre for Nanotechnology, and School of Physics, UoH for Raman and TEM facilities.

Appendix A. Supplementary material

Supplementary data associated with this article can be found, in the online version, at <http://dx.doi.org/10.1016/j.cplett.2017.07.043>.

References

- [1] J.P. Hutchinson, C.J. Evenhuis, C. Johns, A.A. Kazarian, M.C. Breadmore, M. Macka, E.F. Hilder, R.M. Guijt, G.W. Dincoski, P.R. Haddad, Identification of inorganic improvised explosive devices by analysis of postblast residues using portable capillary electrophoresis instrumentation and indirect photometric detection with a light-emitting diode, *Anal. Chem.* 79 (18) (2007) 7005.
- [2] A. Hakonen, F.-C. Wang, P.O. Andersson, H. Wingfors, T. Rindzevicius, M.S. Schmidt, V.R. Soma, S. Xu, Y. Li, A. Boisen, Handheld femtogram detection of hazardous Picric acid with hydrophobic Ag nanopillar SERS substrates and mechanism of elasto-capillarity, *ACS Sens.* 2 (2) (2017) 198.
- [3] S. Wallin, A. Pettersson, H. Östmark, A. Hobro, Laser-based standoff detection of explosives: a critical review, *Anal. Bioanal. Chem.* 395 (2) (2009) 259.
- [4] L. McNesby, A.W. Miziolek, *Laser-based Detection Methods of Explosives*, in: Jehuda Yinon (Ed.), Elsevier, 2011, p. 279.
- [5] B. Sharma, R.R. Frontiera, A.-I. Henry, E. Ringe, R.P. Van Duyne, SERS: materials, applications, and the future, *Mater. Today* 15 (1) (2012) 16.
- [6] A. Chou, E. Jaatinen, R. Buividas, G. Seniutinas, S. Juodkazis, E.L. Izake, P.M. Fredericks, SERS substrate for detection of explosives, *Nanoscale* 4 (23) (2012) 7419.
- [7] S. Hamad, G.K. Podagatlapalli, M.A. Mohiddin, V.R. Soma, Cost effective nanostructured copper substrates prepared with ultrafast laser pulses for explosives detection using surface enhanced Raman scattering, *Appl. Phys. Lett.* 104 (26) (2014) 263104.
- [8] G.K. Podagatlapalli, S. Hamad, S. Venugopal Rao, Trace-level detection of secondary explosives using hybrid silver-gold nanoparticles and nanostructures achieved with femtosecond laser ablation, *J. Phys. Chem. C* 119 (29) (2015) 16972.
- [9] M. Moskovits, Surface-enhanced Raman spectroscopy: a brief retrospective, *J. Raman Spectrosc.* 36 (6–7) (2005) 485.
- [10] A. Campion, P. Kambhampati, Surface-enhanced Raman scattering, *Chem. Soc. Rev.* 27 (4) (1998) 241.
- [11] L. Polavarapu, L.M. Liz-Marzán, Towards low-cost flexible substrates for nanoplasmonic sensing, *Phys. Chem. Chem. Phys.* 15 (15) (2013) 5288.
- [12] H.J. Yin, Y.F. Chan, Z.L. Wu, H.J. Xu, Si/ZnO nanocomb arrays decorated with Ag nanoparticles for highly efficient surface-enhanced Raman scattering, *Opt. Lett.* 39 (14) (2014) 4184.
- [13] L. Jiang, D. Ying, X. Li, Y. Lu, Two-step femtosecond laser pulse train fabrication of nanostructured substrates for highly surface-enhanced Raman scattering, *Opt. Lett.* 37 (17) (2012) 3648.
- [14] D. Zhang, B. Gökce, S. Barcikowski, Laser synthesis and processing of colloids: fundamentals and applications, *Chem. Rev.* 117 (5) (2017) 3990.
- [15] P.A. Mosier-Boss, Review of SERS substrates for chemical sensing, *Nanomaterials* 7 (6) (2017) 142.
- [16] T.E. Itina, On nanoparticle formation by laser ablation in liquids, *J. Phys. Chem. C* 115 (12) (2010) 5044.
- [17] V. Amendola, S. Polizzi, M. Meneghetti, Laser ablation synthesis of gold nanoparticles in organic solvents, *J. Phys. Chem. B* 110 (14) (2006) 7232.
- [18] G. Krishna Podagatlapalli, S. Hamad, S.P. Tewari, S. Sreedhar, M.D. Prasad, S. Venugopal Rao, Silver nano-entities through ultrafast double ablation in aqueous media for surface enhanced Raman scattering and photonics applications, *J. Appl. Phys.* 113 (7) (2013) 073106.
- [19] S. Hamad, G.K. Podagatlapalli, V. Vendamani, S. Nageswara Rao, A. Pathak, S.P. Tewari, S. Venugopal Rao, Femtosecond ablation of silicon in acetone: tunable photoluminescence from generated nanoparticles and fabrication of surface nanostructures, *J. Phys. Chem. C* 118 (13) (2014) 7139.
- [20] S. Venugopal Rao, G.K. Podagatlapalli, S. Hamad, Ultrafast laser ablation in liquids for nanomaterials and applications, *J. Nanosci. Nanotechnol.* 14 (2) (2014) 1364.
- [21] B. Tangeysh, K.M. Tibbetts, J.H. Odhner, B.B. Wayland, R.J. Levis, Gold nanotriangle formation through strong-field laser processing of aqueous KAuCl_4 and postirradiation reduction by hydrogen peroxide, *Langmuir* 33 (1) (2017) 243.
- [22] J. Neddersen, G. Chumanov, T.M. Cotton, Laser ablation of metals: a new method for preparing SERS active colloids, *Appl. Spectrosc.* 47 (12) (1993) 1959.
- [23] J. Kneipp, X. Li, M. Sherwood, U. Panne, H. Kneipp, M.I. Stockman, K. Kneipp, Gold nanolenses generated by laser ablation-efficient enhancing structure for surface enhanced Raman scattering analytics and sensing, *Anal. Chem.* 80 (11) (2008) 4247.
- [24] F. Bertorelle, M. Ceccarello, M. Pinto, G. Fracasso, D. Badocco, V. Amendola, P. Pastore, M. Colombatti, M. Meneghetti, Efficient AuFeO_x nanoclusters of laser-ablated nanoparticles in water for cells guiding and surface-enhanced resonance Raman scattering imaging, *J. Phys. Chem. C* 118 (26) (2014) 14534.
- [25] S. Scaramuzza, D. Badocco, P. Pastore, D.F. Coral, M.B. Fernández van Raap, V. Amendola, Magnetically assembled SERS substrates composed of iron-silver nanoparticles obtained by laser ablation in liquid, *ChemPhysChem* 18 (9) (2017) 1026.
- [26] A. Serkov, E. Barmina, P. Kuzmin, G. Shafeyev, Self-assembly of nanoparticles into nanowires under laser exposure in liquids, *Chem. Phys. Lett.* 623 (2015) 93.
- [27] D. Liu, C. Li, F. Zhou, T. Zhang, H. Zhang, X. Li, G. Duan, W. Cai, Y. Li, Rapid synthesis of monodisperse Au nanospheres through a laser irradiation-induced shape conversion, self-assembly and their electromagnetic coupling sers enhancement, *Sci. Rep.* 5 (2015) 7686.
- [28] R. Torres-Mendieta, D. Ventura-Espinosa, S. Sabater, J. Lancis, G. Mínguez-Vega, J.A. Mata, In situ decoration of graphene sheets with gold nanoparticles synthesized by pulsed laser ablation in liquids, *Sci. Rep.* 6 (2016).
- [29] A. Wang, L. Jiang, X. Li, Q. Xie, B. Li, Z. Wang, K. Du, Y. Lu, Low-adhesive superhydrophobic surface-enhanced Raman spectroscopy substrate fabricated by femtosecond laser ablation for ultratrace molecular detection, *J. Mater. Chem. B* 5 (4) (2017) 777.
- [30] C. Noguez, Surface plasmons on metal nanoparticles: the influence of shape and physical environment, *J. Phys. Chem. C* 111 (10) (2007) 3806.
- [31] K.A. Willets, R.P. Van Duyne, Localized surface plasmon resonance spectroscopy and sensing, *Annu. Rev. Phys. Chem.* 58 (2007) 267.
- [32] M.A. Sobhan, M. Ams, M.J. Withford, E.M. Goldys, Ultrafast laser ablative generation of gold nanoparticles: the influence of pulse energy, repetition frequency and spot size, *J. Nanopart. Res.* 12 (8) (2010) 2831.
- [33] A. Serkov, M. Shcherbina, P. Kuzmin, N. Kirichenko, Laser-induced agglomeration of gold nanoparticles dispersed in a liquid, *Appl. Surf. Sci.* 336 (2015) 96.
- [34] A. Vorobyev, C. Guo, Multifunctional surfaces produced by femtosecond laser pulses, *J. Appl. Phys.* 117 (3) (2015) 033103.
- [35] A.Y. Vorobyev, C. Guo, Direct femtosecond laser surface nano/microstructuring and its applications, *Laser Photon. Res.* 7 (3) (2013) 385.
- [36] J. Fujimoto, J. Liu, E. Ippen, N. Bloembergen, Femtosecond laser interaction with metallic tungsten and nonequilibrium electron and lattice temperatures, *Phys. Rev. Lett.* 53 (19) (1984) 1837.
- [37] E. Le Ru, E. Blackie, M. Meyer, P.G. Etchegoin, Surface enhanced Raman scattering enhancement factors: a comprehensive study, *J. Phys. Chem. C* 111 (37) (2007) 13794.
- [38] H. He, W. Cai, Y. Lin, B. Chen, Au nanochain-built 3D netlike porous films based on laser ablation in water and electrophoretic deposition, *Chem. Commun.* 46 (38) (2010) 7223.
- [39] G.-N. Xiao, S.-Q. Man, Surface-enhanced Raman scattering of methylene blue adsorbed on cap-shaped silver nanoparticles, *Chem. Phys. Lett.* 447 (4) (2007) 305.
- [40] R.R. Naujok, R.V. Duevel, R.M. Corn, Fluorescence and Fourier transform surface-enhanced Raman scattering measurements of methylene blue adsorbed onto a sulfur-modified gold electrode, *Langmuir* 9 (1993) 1771.
- [41] C. Wang, B. Liu, X. Dou, Silver nanotriangles-loaded filter paper for ultrasensitive SERS detection application benefited by interspacing of sharp edges, *Sens. Actuators B: Chem.* 231 (2016) 357.
- [42] K. Kosuda, J. Bingham, K. Wustholz, R. Van Duyne, Nanostructures and surface-enhanced Raman spectroscopy, *Handbook of Nanoscale Optics and Electronics*, 2010, p. 309.
- [43] M.E. Farrell, E.L. Holthoff, P.M. Pellegrino, Surface-enhanced Raman scattering detection of ammonium nitrate samples fabricated using drop-on-demand inkjet technology, *Appl. Spectrosc.* 68 (3) (2014) 287.
- [44] M. Guo, Y. Zhao, C. Feng, S. Li, Y. Jiang, Surface and shape unification of excimer pulse irradiated Ag nanoparticles and associated surface-enhanced Raman scattering properties, *J. Laser Appl.* 29 (2) (2017) 022006.
- [45] W. Du, L. Liu, P. Gu, J. Hu, P. Zhan, F. Liu, Z. Wang, Hotspot-engineered quasi-3D metallic network for surface-enhanced Raman scattering based on colloid monolayer templating, *Appl. Phys. Lett.* 109 (12) (2016) 121108.
- [46] M.E. Farrell, P. Strobbia, P.M. Pellegrino, B. Cullum, Surface regeneration and signal increase in surface-enhanced Raman scattering substrates, *Appl. Opt.* 56 (3) (2017) B198.
- [47] S. Botti, L. Cantarini, S. Almaviva, A. Puiu, A. Rufoloni, Assessment of SERS activity and enhancement factors for highly sensitive gold coated substrates probed with explosive molecules, *Chem. Phys. Lett.* 592 (2014) 277.
- [48] A. Hakonen, P.O. Andersson, M.S. Schmidt, T. Rindzevicius, M. Käll, Explosive and chemical threat detection by surface-enhanced Raman scattering: a review, *Anal. Chim. Acta* 893 (2015) 1.
- [49] Z.M. Jin, W. Gu, X.B. Shi, Z.K. Wang, Z.Q. Jiang, L.S. Liao, A novel route to surface-enhanced Raman scattering: Ag nanoparticles embedded in the nanogaps of a Ag substrate, *Adv. Opt. Mater.* 2 (6) (2014) 588.
- [50] G.K. Podagatlapalli, S. Hamad, M.A. Mohiddin, S.V. Rao, Fabrication of nanoparticles and nanostructures using ultrafast laser ablation of silver with Bessel beams, *Laser Phys. Lett.* 12 (3) (2015) 036003.